AMERICAN
METEOROLOGICAL
SOCIETY

Journal of Climate

EARLY ONLINE RELEASE

This is a preliminary PDF of the author-produced manuscript that has been peer-reviewed and accepted for publication. Since it is being posted so soon after acceptance, it has not yet been copyedited, formatted, or processed by AMS Publications. This preliminary version of the manuscript may be downloaded, distributed, and cited, but please be aware that there will be visual differences and possibly some content differences between this version and the final published version.

The DOI for this manuscript is doi: 10.1175/JCLI-D-13-00269.1

The final published version of this manuscript will replace the preliminary version at the above DOI once it is available.

If you would like to cite this EOR in a separate work, please use the following full citation:

Kiranmayi, L., L. Leung, S. Hagos, V. Vinoj, S. Rauscher, T. Ringler, and M. Taylor, 2013: The dependence of ITCZ structure on model resolution and dynamical core in aqua-planet simulations. J. Climate. doi:10.1175/JCLI-D-13-00269.1, in press.

© 2013 American Meteorological Society

Manuscript (non-LaTeX)
Click here to download Manuscript (non-LaTeX): Kiran_etal_itcz_revized_final_oct1.docx

PRELIMINARY ACCEPTED VERSION

The dependence of ITCZ structure on model resolution and dynamical core in aqua-planet simulations

Kiranmayi Landu[1a], L. Ruby Leung[1], Samson Hagos[1], V. Vinoj[1], Sara A. Rauscher[2], Todd Ringler[2], and Mark Taylor[3]

[1]*Pacific Northwest National Laboratory*

[2]*Los Alamos National Laboratory*

[3]*Sandia National Laboratory*

[a]*Corresponding author email: Kiranmayi.Landu@pnnl.gov*

Submitted May 2013

Revised October 2013

Abstract

Aqua-planet simulations using the Community Atmosphere Model version 4 (CAM4) with the Model for Prediction Across Scales - Atmosphere (MPAS-A) and Higher Order Method Modeling Environment (HOMME) dynamical cores and zonally symmetric sea surface temperature (SST) structure are studied to understand the dependence of the inter-tropical convergence zone (ITCZ) structure on resolution and dynamical core. While all resolutions in HOMME and the low-resolution MPAS-A simulations give a single equatorial peak in zonal mean precipitation, the high-resolution MPAS-A simulations give a double ITCZ with precipitation peaking around 2° to 3° on either side of the equator. This study reveals that the structure of ITCZ is dependent on the feedbacks between convection and large-scale circulation. We show that difference in specific humidity between HOMME and MPAS-A can lead to different latitudinal distributions of the convective available potential energy (CAPE) by influencing latent heat release by clouds and the upper tropospheric temperature. With lower specific humidity, the high resolution MPAS-A simulation has CAPE that increases away from the equator that enhances convection away from the equator and through a positive feedback on the circulation, results in a double ITCZ structure. We further show that the dominance of anti-symmetric waves in the model is not enough to cause double ITCZ, and the lateral extent of equatorial waves does not play an important role in determining the width of the ITCZ but rather the latter may influence the former.

1. Introduction

The Inter-tropical convergence zone (ITCZ) is the belt of east – west oriented high precipitation region observed over the tropics. Climatologically, the zonal mean ITCZ is located slightly to the north of the equator. Simulation of the ITCZ in general circulation models is one of the most challenging aspects of modeling (e.g. Neelin et al. 1992, Lin 2007). Simulations of ITCZ show two prevalent structures: a single ITCZ that peaks to the north of the equator or double ITCZs with peaks of precipitation on either side of the equator (Zhang and Wang 2006, Lin 2007, Zhang et al. 2007, Liu et al. 2010). Most climate models show a second precipitation belt over the southern hemisphere especially in the Pacific, giving a double peak structure when zonally averaged (Lin 2007). The double ITCZ structure also manifests in atmospheric models without ocean coupling, suggesting the primary role of atmospheric dynamics in generating the double ITCZ. This prevalence of 'double ITCZ syndrome' in models is an important model bias in the simulation of not only the tropics but also general circulation. Even models run in idealized aqua-planet configuration showed both single and double ITCZ structures (e.g. Numaguti 1993, Chao and Chen 2004, Liu and Moncrieff 2008, Liu et al. 2010, Mobis and Stevens 2012, Oueslati and Bellon 2012,). Zonally symmetric model configurations are also shown to simulate single (with precipitation peak centered on equator) or double ITCZ (with peaks on either side of the equator) and even asymmetric ITCZ with a single precipitation belt peaking off the equator when uniform SST is prescribed (e.g. Chao and Chen 2004).

Different hypotheses have been proposed to explain the double ITCZ in models. Many factors such as SST gradient (e.g. Oueslati and Bellon 2012), cumulus parameterization (e.g. Liu et al. 2010), and model resolution (e.g. Williamson 2008) have been documented to influence the structure of the ITCZ. Some of the initial studies proposed the CISK (convective instability of the second kind) mechanism to explain the ITCZ splitting (e.g. Charney 1971, Lindzen 1974). Influence of wind induced surface heat exchange is shown to be another important factor affecting the location of the ITCZ (e.g. Liu et al. 2010, Liu and Moncrieff 2004, Liu and Moncrieff 2008). Chao and Chen (2004) show that there are two forces acting to attract ITCZ towards and away from the equator, namely Coriolis force and convective circulation modified by Coriolis force. The feedback between convection and large-scale circulation is another phenomenon suggested to be important in deciding the single and double structure of ITCZ (e.g. Horinouchi 2012, Oueslati and Bellon 2012, Mobis and Stevens 2012). The position of ITCZ is also influenced by exra-tropical clouds and ice (e.g. Chiang et al. 2003, Frierson and Hwang 2012). Some studies have also demonstrated how equatorial waves increase the chance of double ITCZ in the model by modulating the organized convection into symmetric and anti-symmetric waves (e.g. Abiodun et al. 2008, Horinouchi 2012). Abiodun et al. (2008) explain that at higher resolutions equatorial waves are better simulated and precipitation corresponding to equatorial (anti-symmetric) wave peaks off-equator, resulting in double ITCZ.

In spite of these previous studies, there is still a lack of a coherent theory that can explain the change between single and double ITCZ in climate models. The explanations so far seem to be largely model dependent and/or parameterization dependent. In the

absence of a unified explanation, it is important to understand the reasons behind the simulated ITCZ structure differences in each model to understand the tropical biases. Because of the simplicity of the forcings involved (such as absence of land-sea contrast, orography), simulations with zonally symmetric aqua-planet model configuration are useful for studying the differences between the dynamical processes causing single and double ITCZ.

In this study, we examine the structure of ITCZ in two sets of aqua-planet simulations produced by two different dynamical cores within the Community Atmosphere Model Version 4 (CAM4, Neale et al. 2010), namely the Model for Prediction Across Scales - Atmosphere (MPAS-A) (Rauscher et al. 2012) and the High-Order Method Modeling Environment (HOMME, Taylor et al. 2008), each performed at 4 different horizontal resolutions ranging from about 0.25^{o} to 2°. CAM4 is run with these two dynamical cores following the aqua-planet experiment protocol described by Neale and Hoskins (2000) with the same physics parameterizations. Both MPAS-A and HOMME simulate maximum precipitation over the tropical region forming an ITCZ like structure. Figure 1 shows the latitudinal distribution of zonal mean total precipitation for both models at different resolutions. Although both models use the same physics package including convective parameterizations, MPAS-A at higher resolutions generate a double ITCZ-like pattern whereas in the HOMME simulations, a single narrow precipitation band is maintained at all four resolutions. The objective of this study is to examine the factors influencing the double and single ITCZ structures simulated by these models. We explore the roles of equatorial waves, and convection and large scale circulation feedbacks in determining the structure of ITCZ in these models. Section 2 decribes the

model configurations, section 3 presents the results from various analyses, followed by conclusions in section 4.

2. Model Description

We use outputs from aqua-planet simulations of CAM generated by MPAS-A (Skamarock et al. 2012) and HOMME (Taylor et al. 2008). MPAS-A uses unstructured Voronoi meshes and C-grid discretization as the basis of the model components. The unstructured Voronoi meshes allow for both quasi-uniform discretization of the sphere and local refinement (Du et al. 1999; Ringler et al. 2008; Ju et al. 2011). The underlying numerical method used in MPAS-A is described in Thuburn et al. (2009) and Ringler et al. (2010). In this study, MPAS-A is run with quasi-uniform resolutions of 240km, 120km, 60km and 30km. Further details about model configurations for these experiments are discussed in Rauscher et al. (2012).

HOMME uses spectral finite element discretization on relatively isotropic cubed sphere grid (Taylor et al. 2008; Evans et al. 2013). The HOMME spectral element discretization uses a compatible formulation that conserves dry mass and total energy and has significantly improves scaling as compared to the CAM finite volume and spectral Eulerian dynamical cores (Dennis et al. 2012). HOMME simulations are run at resolutions comparable to MPAS-A at 220km, 120km, 55km and 28km. Following the aqua-planet experiment protocol of Neale and Hoskin (2000) all simulations are run with zonally symmetric fixed sea surface temperature, which is also symmetrical about the equator. In addition, solar insolation is fixed at the March equinoctial condition, which is symmetric about the equator. Hence any response not symmetric about the equator can

only arise from internal model variability. Note that we use the same CAM4 physics package in both sets of simulations. A physics time step of 10 minutes is used and all physics parameter settings are the same in all simulations – i.e., no tuning was performed at different resolutions. In the present study, precipitation, winds, temperature, specific humidity, surface flux and surface pressure data with output every 6 hours and their monthly averages are used. The models are run for 5 years, but only data for the last 4 years are used in the analyses.

In the following sections, we mainly compare results from simulations of MPAS-A at 240 km resolution (denoted as M240) and MPAS-A at 30km (denoted as M30) to understand the effect of resolution and use M30 and HOMME at 28km resolution (denoted as H28) to compare the effect of dynamical core.

3 Results

a) Convection feedbacks

The precipitation over a region is determined by the total available moisture in the column and the parameterizations used by the model. Column integrated moisture budget analysis provides an excellent means of understanding different factors contributing to precipitation over a region. This is expressed by the following equation,

$$\langle \frac{\partial q}{\partial t} \rangle = -\langle V.\nabla q \rangle - \langle \omega \frac{\partial q}{\partial p} \rangle + E - P$$

where q is specific humidity, V is horizontal component of wind velocity, ω is vertical pressure velocity, E and P are evaporation and precipitation respectively. Parentheses < > represent vertical integration from surface to the top of the atmosphere. The left hand side

of the equation is zero when the system is in steady state averaged over a long period. On the right hand side, the first two terms correspond to horizontal and vertical advection of moisture. Figure 2 shows the zonal mean distribution of precipitation, evaporation and the advection terms (horizontal and vertical combined) from the above equation for the MPAS-A low resolution (M240), MPAS-A high resolution (M30) and equivalent HOMME high resolution (H28) simulations. Over the tropics, the dominant contribution to precipitation comes from advection. The distribution of evaporation is almost identical in all simulations, while the shape of the advection terms is responsible for the ITCZ structure simulated.

Among the advection terms, the dominant contribution comes from vertical advection given by $\langle \omega \frac{\partial q}{\partial p} \rangle$ whereas horizontal advection is an order of magnitude smaller. The structure of vertical advection is similar to the total advection, with a distinct double peak in M30 coinciding with the double peaks in precipitation (figure not shown). The magnitude of this term is higher in H28 compared to MPAS-A simulations. Figure 3 shows the distribution of vertical pressure velocity in the three simulations. The latitudinal distributions of vertical winds in the three simulations almost resemble that of precipitation with M30 showing two peaks and H28 and M240 showing a single equatorial peak. Even the differences in the amplitudes of vertical winds among the simulations compare fairly similarly to the differences of precipitation. That is, similar to HOMME producing much higher precipitation amounts concentrated over a narrower belt centered over the equator, the updrafts in HOMME are far higher and concentrated closer to the equator compared to MPAS-A.

In the tropics, the main factor contributing to the updraft speeds is the latent heat release by cloud condensation. This released latent heat increases the buoyancy of the parcel, intensifying the updrafts. Since convection is a dominant process for cloud formation in the tropics, the cumulus parameterization may play an important role in determining the latent heat release and updraft speed. In the present model, the modified version of Zhang and McFarlane (Zhang and McFarlane 1995) scheme is used to parameterize convection. This scheme uses a threshold in CAPE (70J kg^{-1}) to trigger moist convection. Figure 4 shows the distribution of zonal mean CAPE for the three simulations. CAPE increases with resolution in MPAS-A. M30 has higher CAPE compared to H28 and the latitudinal extent is larger. The zonal mean CAPE has a similar distribution as that of precipitation and updraft speed with double peaks in M30 coinciding with the peaks in precipitation. On average, threshold values of CAPE are reached beyond 5° of latitudes in M30, whereas in H28, these values are present over a narrower range of latitudes of about 3° from the equator. In the MPAS-A simulations, CAPE decreases with decreased resolution. The overall values of CAPE in M240 are far smaller compared to the other two simulations with threshold values reached only in a narrow region towards the equator.

Having established the similarity between the latitudinal distribution of precipitation with that of updraft speed and CAPE, it is important to understand the factors contributing to the shapes and magnitudes of the latter. CAPE represents the buoyancy of an air parcel, and is determined largely by atmospheric stability or the moist static energy profile, which depends on the temperature and humidity profiles. To understand the factors leading to higher CAPE over a wider area in MPAS-A compared

to HOMME, Figure 5 shows the vertical temperature and specific humidity differences between H28 and M30. The HOMME simulation has higher specific humidity compared to MPAS-A. Furthermore, H28 has higher temperature compared to M30 at all levels except above 100mb, and the difference increases with altitude to reach 3K around 150mb in the upper troposphere. Near the surface, the temperature difference is small as both simulations are constrained by the same prescribed SST. With higher specific humidity and comparable temperature at low levels, HOMME has higher moist static energy than MPAS-A. However, at upper levels, larger increase in temperature with altitude in H28 results in increased atmospheric stability compared to MPAS-A so HOMME has lower CAPE values than MPAS-A, except very close to the equator (Figure 4).

Because of higher specific humidity, more latent heat is released in H28 compared to M30 when CAPE is above the threshold, which happens on average roughly between 3°N and 3°S. This region coincides with the latitudinal belt at which H28 has higher precipitation than H28. The higher cloud latent heat release in H28 contributes to a warmer poleward branch of the Hadley circulation. This contributes to the warmer temperature in the upper troposphere in H28 compared to M30. Hence the increased specific humidity towards the equator plays a major role in determining the CAPE in HOMME by increasing latent heat release near the equator and poleward heat transport. The latter results in warmer upper tropospheric temperature, which increases atmospheric stability and reduces CAPE poleward, giving rise to a narrower CAPE distribution and precipitation belt. Compared to H28, M30 has lower latent heat release because of the lower specific humidity. Because of the reduced poleward heat transport, the upper

tropospheric temperature is lower so vertical stability is reduced in the atmospheric column further away from the equator. This results in higher CAPE values and latent heat release away from the equator.

To determine the factors contributing to the CAPE difference in MPAS-A at low and high resolution, we note that in M240, both vertical winds and specific humidity are comparable to M30 (figure not shown), so the mechanisms leading to differences between H28 and M30 are not likely to be responsible for the differences between M240 and M30. Further analyses show that the distribution of cloud amount varies with resolution. Figure 6 shows the zonal mean cloud fraction in M30 and M240. By comparing the distribution of cloud amount in these two resolutions, it is clear that M240 has more cloud amount and the difference is larger at the upper troposphere compared to mid troposphere. This increases the relative magnitude of upper tropospheric cloud and latent heat release that result in increased poleward heat transport, increased atmospheric stability, and reduced CAPE. The preference for high clouds in the low resolution simulations is consistent with O'Brien et al. (2013), who found that the cloud size in CAM4 aqua-planet simulations decreases with increase in resolution. Low resolution simulations have larger clouds that result mainly from large scale condensation, since the CAPE values in M240 are much lower than M30 and barely above the threshold used in the cumulus parameterization (Figure 4). As the maximum altitude of clouds increases with increased cloud size (e.g Wilcox and Ramanathan 2001), the increased upper tropospheric cloud fraction contributes to increased upper tropospheric temperatures relative to high resolution and reduces atmospheric stability poleward.

Having elucidated the differences in CAPE among the simulations, we return to the moisture budget that directly attributes precipitation to its moisture sources. From Figure 2, it is seen that the main source of moisture for precipitation in both HOMME and MPAS-A is vertical advection. From the continuity equation and integration by parts, this term is equal to the advection of moisture through horizontal wind divergence, expressed as $\int q\nabla.V$. In the present zonally symmetric aqua-planet model, zonal advection is negligible when taking the zonal mean profiles. This implies that the meridional wind divergence is one of the main contributors in modulating the precipitation patterns in our simulations. As the meridional winds transport moisture towards the equator and reach the latitudes where CAPE exceeds the threshold values, moist convection is triggered. The latitude at which this triggering happens is farther from the equator in M30 compared to HOMME or the lower resolution MPAS-A simulations because M30 has higher CAPE values over a broader range of latitudes for reasons discussed earlier. This triggered condensation increases the instability of the column by release of latent heating at the upper troposphere (CISK mechanism), causing increased vertical velocities at these latitudes. Hence, the latitudinal distribution of vertical velocity in Figure 3 is similar to that of precipitation with a maximum in wind speed coinciding with the location of peak precipitation corresponding to each simulation. As can be seen from the figure, stronger negative velocities start to develop farther away from the equator in MPAS-A compared to HOMME. Consequently, increased vertical winds off the equator cause an increased transport of moisture into the upper troposphere and decreased pressure, leading to lateral expansion of the lower pressure gradient. This shifts the region of large pressure gradient away from the equator

and feeds back positively to increase convergence over the region. Reduced pressure gradient and the associated wind speeds on the equator side of this latitude lead to a consequent dip in specific humidity being transported towards the equator. This results in a decrease of CAPE and moisture supply over the equator, and hence lowers precipitation over the equator causing the double peak in precipitation. The positive feedback between condensation and moisture convergence contributes to the much larger differences in precipitation and updraft speeds (Figure 3) than CAPE (Figure 4) among the simulations, although these quantities all share similar latitudinal distributions.

In the lower resolution MPAS-A simulation, the magnitude of specific humidity and hence CAPE is smaller. Hence precipitation triggering is only possible at latitudes closer to the equator leading to single ITCZ structure. Although the cloud amounts in M240 are large (Figure 6), they are mostly associated with large-scale condensation that does not produce as significant precipitation as convection that dominates in M30 and H28.

b) Effect of equatorial waves

Previous studies have shown the importance of equatorial waves on the ITCZ structure. For example, Abiodun et al. (2008) showed that simulation of equatorial waves at higher resolutions contributed to double ITCZ in contrast to single ITCZ in lower resolutions. Honirouchi (2012) showed the effect of equatorial waves on Hadley circulation and ITCZ structure. Most of the tropical waves have a dynamical structure with precipitation peak occurring on either side of the equator. Such waves include all asymmetric waves and also symmetric waves like Rossby waves and even-mode Inertio Gravity (IG) waves. On the other hand, symmetric waves like Kelvin waves have

corresponding precipitation peak centered over the equator, facilitating a single ITCZ structure. We study the effect of these waves simulated in the present models on the ITCZ.

Wavenumber – frequency spectra of precipitation calculated using the Wheeler and Kiladis (1999) method show that MPAS-A and HOMME both simulate Kelvin, Rossby and IG waves (Rauscher et al. 2012). Wavenumber frequency filtering of precipitation corresponding to different theoretical wave regimes allows a comparison of the wave amplitude variations in the simulations. We follow Wheeler and Kiladis (1999) to calculate the wave amplitudes in order to examine the latitudinal variation of amplitudes corresponding to different waves. The equivalent depths used for filtering in the present study are 15m and 75m as most of the wave amplitude falls within this region.

The analysis shows that for all waves at all resolutions, the HOMME simulations have higher amplitude compared to MPAS-A (figure not shown). However, the magnitudes of the waves are mainly determined by the magnitude of the precipitation itself. To understand the relative importance of different waves in these simulations, we look at the ratio of Kelvin wave amplitude to asymmetric wave amplitudes in each model (Figure 7). A higher value of this ratio should favor single ITCZ while a lower value should favor double ITCZ structure. In both models, the ratio decreases with increasing resolution, showing higher possibility of double peaks at higher resolutions. However MPAS-A has a higher ratio compared to HOMME except at the highest resolution, which is inconsistent with the nature of the ITCZ structure simulated by M30 where double ITCZ is most apparent. From this we conclude that the dominance of different types of waves simulated alone do not determine the structure of ITCZ in these simulations or it

may play a more minor role that is overshadowed by the CAPE and convection feedback mechanisms discussed above.

Another factor that can influence ITCZ structure is the distance of the precipitation peak from the equator. From equatorial wave theory, the distance of the peak from the equator depends on the latitudinal extent of the waveguide given by the expression

$y_c^2=(2n+1)c/\beta$

where y_c represents the latitudinal extent, n is the meridional mode number of the wave, c is gravity wave speed given by $\sqrt{gh_{eq}}$ where h_{eq} is the equivalent depth of the atmosphere and β is the Coriolis constant. In this equation, the only variable is the gravity wave speed, which depends on the equivalent depth h_{eq} of the system. The equivalent depth can further be determined using the expression given by Tian and Ramanathan (2003) as

$$h_{eq} = \frac{R_d \Delta m \Delta p}{4gC_p P_m} = \frac{R_d \Delta m}{4gC_p}\left(1 - \frac{p_d}{p_m}\right)$$

where R_d is the gas constant, Δm is gross moist stability, p_m is the level at which the divergence changes sign, and Δp is the depth between p_m and the level of upper tropospheric divergence maximum (p_d). From this equation, variables that can change the equivalent depth are Δm, p_d and p_m. Increase in Δm and p_m leads to increased h_{eq} and increased p_d leads to decreased h_{eq}. In the present models, the ratio $\frac{p_d}{p_m}$ is almost constant. Hence the only contributing term is the gross moist stability of the system. Here we calculate the gross moist stability following Neelin and Held (1987) and equations 3 and 4 in Frierson (2007). Figure 8 shows the zonal mean Gross Moist Stability (GMS)

divided by C_p at the equator for both models at different resolutions. In both models, there is a monotonic decrease in GMS with resolution. This should actually result in narrowing of the wave lateral width at higher resolution. But a comparison of the distance of peak wave amplitudes shows that in MPAS-A the waves are laterally wider at higher resolutions whereas in HOMME the distance decreases, which is inconsistent with the observed GMS values. This means that the width of the wave is modulated by the width of the ITCZ itself. From this it can be inferred that the simulated characteristics of the equatorial waves in the models are dependent on the ITCZ structure, rather than the waves influencing the structure of the ITCZ in contrast to the findings of Abiodun et al. (2008).

4 Discussion

Although many studies have addressed the ITCZ structure in aqua-planet simulations and investigated the factors affecting single/double ITCZ, the mechanisms determining ITCZ splitting are still ambiguous. Here we look at two dynamical frameworks with similar configurations in idealized aqua-planet simulations to understand how the simulated large scale environments and equatorial waves modulate the ITCZ structure in these models. Despite the common physics parameterizations used in both MPAS-A and HOMME, the ITCZ structures simulated by the models are different with MPAS-A displaying double ITCZ at higher resolutions while HOMME showing a consistent narrow single ITCZ regardless of resolution.

Analyzing different factors affecting the structure of the ITCZ in these simulations, we show that the feedbacks between convection and large-scale Hadley circulation determine whether the model simulation will have single or double ITCZ. In

HOMME, higher specific humidity results in higher latent heat release in convective clouds. The energy is transported poleward by the Hadley circulation and increases the upper tropospheric temperature in HOMME relative to MPAS-A and decreases CAPE poleward. This limits convective precipitation closer to the equator, resulting in narrower albeit higher precipitation because of the higher specific humidity, giving rise to a single ITCZ. On the other hand, in MPAS, at higher resolution (M30), the zonal mean CAPE is higher farther away from the equator as lower specific humidity reduces the poleward heat transport by the Hadley circulation and the lower upper tropospheric temperature compared to H28 enhances atmospheric instability poleward and triggers a wider precipitation band.

In both HOMMA and MPAS-A, the increased precipitation at or away from the equator enhances vertical winds through latent heat release. This consequently further enhances surface convergence over the respective regions. In M30, this increased convergence away from equator causes reduced moisture being transported towards the equator-side. This dip in moisture and the resulting reduction in CAPE cause a dip in the precipitation at the equator, resulting in a double ITCZ structure in the simulation. In contrast, when MPAS-A is applied at coarser resolution (M240), the preference for high-level clouds compared to M30 results in top-heavy temperature profiles and reduced CAPE so that convection can only be triggered close to the equator, leading to a single ITCZ. We note, however, that M240 simulates a larger amount of clouds compared to M30, but the clouds are primarily associated with large-scale condensation since CAPE values are very low in M240. A flow chart of feedbacks leading to single and double ITCZ structures in HOMME and MPAS-A at high resolution is given in Figure 9.

The role of equatorial waves in modulating the ITCZ structure is also explored in these simulations. We show that the dominance of asymmetric waves is not enough to cause a split in the ITCZ in our simulations. This can happen because a large portion of precipitation variability is not organized by the equatorial waves; hence the zonal mean precipitation features are primarily attributed to the red-noise. In the present simulations, convectively coupled equatorial waves are not discernable from the raw spectra proving that the precipitation is dominated by processes associated with the red-noise. We also investigate the factors affecting the lateral extent of equatorial waves. Although the equivalent depth of the system decreases with resolution in MPAS-A, the width of equatorial waves still increases with increased resolution. This shows that the lateral extent of the waves may be determined by the width of the ITCZ precipitation (which is governed more by the red-noise) rather than the wave width determining the ITCZ.

Previous studies have suggested a role for surface fluxes in the single versus double ITCZ structure (e.g., Liu and Moncrieff 2004). In our simulations, higher humidity in HOMME leads to lower surface latent flux compared to MPAS-A, but the differences are relatively small. Because of the lower humidity, the surface latent heat flux in MPAS-A is more sensitive to changes in surface winds, which may contribute to the enhanced vertical moisture transport associated with the enhanced low-level convergence away from the equator in M30 and further accentuate the off equator precipitation peaks. However, as CAPE plays a key role in determining the latitudinal structure of the ITCZ but it is more dominantly influenced by atmospheric stability that depends on the moist static energy profile, the impacts of surface fluxes on the ITCZ would appear to be relatively minor in our simulations.

Another important feature of the double ITCZ structure is the distance of peak precipitation from the equator. Many studies explored various factors contributing to the distance between the ITCZ peaks by varying the SST distribution, convective parameterization, etc. (e.g. Bellon and Sobel 2010). In the present study, the location of peak precipitation is 2° to 3° from equator, which is closer to the equator than most previous studies in which the ITCZs vary between 5° to 15° away from the equator. In the present simulations, the magnitude of CAPE is very low relative to most previous studies. As CAPE decreases poleward, the low CAPE values might be limiting the latitudinal expansion of precipitation zone, thus giving rise to ITCZ bands that are closer to the equator. However, exploring the mechanisms behind this latitudinal extent of ITCZ is beyond our scope and requires further study.

Overall our analyses of aqua-planet simulations produced by MPAS-A and HOMME using the same physics parameterizations at different spatial resolutions suggest that dynamical core and model resolution play a role in the single vs. double ITCZ structure through their influence on the large scale environments including Hadley circulation and humidity. Differences latent heat release by clouds and humidity influence the vertical temperature profile and CAPE and affect convection. The subsequent feedbacks from convection to the large-scale convergence further enhance precipitation off the equator and reduce CAPE and precipitation over the equator, leading to a double ITCZ structure in MPAS-A at higher resolution. Convective parameterizations also play a role in this mechanism through the dependence of convective triggering on CAPE. Convective parameterizations that have stronger dependence on large-scale forcing may be less sensitive to differences in CAPE caused

by differences in dynamical cores and/or model resolutions, hence display different sensitivity of the ITCZ structure to dynamical cores and model resolutions.

Similar ITCZ structures were also studied previously by Williamson and Olson (2003) using two CAM dynamical cores, namely, Eulerian and semi-Lagrangian. They showed that the difference in time-step used in the two dynamical cores results in different moisture deposit from surface fluxes, leading to different CAPE and ITCZ structures. In the present simulations, both dynamical and physics time steps are the same between MPAS-A and HOMME and moisture and precipitation amount is actually higher in the HOMME simulations with a single ITCZ. Thus it appears that even with the same time steps, the numerics of different dynamical cores can result in different humidity states in the models, which favor different kinds of equilibriums leading to contrasting ITCZ structures.

Shorter sensitivity experiments with HOMME including switching from the Eta vertical coordinate (Simmons and Burridge 1981) to a vertical semi-Lagrangian method similar to Lin and Rood (1997), hence adding vertical dissipation to the model, and doubling the surface latent heat flux do not result in a change in the single ITCZ structure. Rauscher et al. (2012) experimented with MPAS-A by reducing the coefficient of the ∇^4 dissipation and found a single ITCZ at high resolution. However the simulation still exhibits a double ITCZ structure in the convective precipitation even though the large scale precipitation is significantly enhanced and its peak over the equator overwhelms the off-equator peaks in the convective precipitation. A detailed investigation of the numerical sources of these differences is beyond the scope of the present study. We show that despite similar model configurations, a change in one of the

basic states (e.g. specific humidity) from differences in the dynamical cores alone can lead to differences in climate processes amplified by positive feedbacks that result in different structures of the salient circulation patterns.

Acknowledgements: This study was funded by the Department of Energy Regional and Global Climate Modeling (RGCM) program through the project "Development of frameworks for robust regional modeling". We thank Prof. Eric D. Maloney of Colorado State University for constructive discussions on analysis of the equatorial waves. We thank Dr. Jin-Ho Yoon for constructive reviews in improving the quality of the manuscript. Thanks also go to Dr. Hui Wan at PNNL for insightful discussions. PNNL is operated by Battelle Memorial Institute for the U.S. Department of Energy under contract DE-AC05-76RLO1830.

References

Abiodun B.J., W.J.Jr. Gutowski, J.M. Prusa , 2008: Implimentation of a non-hydrostatic, adaptive-grid dynamics core in CAM3. Part II: dynamical influence on ITCZ behavior and tropical precipitation. *Clim Dyn*., DOI 10.1007/s00382-008-0382-x

Bellon G., A.H. Sobel, 2010: Multiple equilibria of Hadley circulation in an intermediate-complexity axisymmetric model. *J. Clim.*, **23**, 1760 – 1777.

Chao, W. C., and B. Chen, 2004: Single and double ITCZ in an aqua-planet model with constant sea surface temperature and solar angle. *Climate Dyn*., **22**, 447–459.

Charney, J. G., 1971: Tropical cyclogenesis and the formation of the ITCZ. Mathematical Problems of Geophysical Fluid Dynamics, W. H. Reid, Ed., American Mathematical Society, 355–368.

Chiang, J. C. H., M. Biasutti, and D. S. Battisti, 2003: Sensitivity of the Atlantic ITCZ to Last Glacial Maximum boundary conditions. *Paleoceanography*, **18**, doi:10.1029/2003PA000 916.

Dennis, J., J. Edwards, K.J. Evans, P. Lauritzen, A.A. Mirin, A. St-Cyr, M.A. Taylor, and P.H. Worley, 2012: CAM-SE: A scalable spectral element dynamical core for the Community Atmosphere Model. *Int. J. High Perf. Comput. Appl*., **26**, 74-89.

Du, Q., V. Faber and M. Gunzburger, 1999: Centroidal Voroni tessellations: Aplications and algoritms. *SIAM review*, **41 (4)**, 637-676.

Evans, K.J., P. Lauritzen, S.K. Mishra, R. Neale, M.A. Taylor, and J.J. Tribbia, 2013: AMIP simulations with the CAM4 spectral element dynamical core. *J. Clim*., **26(3)**, 689-709.

Frierson, D.M.W. and Y.T. Hwang, 2012: Extratropical influence on ITCZ shifts in slab ocean simulations of global warming. *J.Climate*, **25**, 720-733.

Ju, L.T., T. Ringler and M. Gunzburger, 2011: Voroni tessellations and their application to climate and global modeling. *Springer Lecture Notes in Computational Science and Engineering*, 1-20

Horinouchi T., 2012: Moist Hadley circulation: Possible role of wave – convection coupling in aquaplanet experiments. *J. Atmos. Science.*, **69**, 891-907.

Lin, J. L., 2007: The double-ITCZ problem in IPCC AR4 coupled GCMs: Ocean–atmosphere feedback analysis. *J. Climate*, **18**, 4497–4525.

Lin, S.-J., and R.B. Rood, 1997: An explicit flux-form semi-Lagrangian shallow-water model on the sphere. *Quart. J. Roy. Meteor. Soc*., **123**, 2477-2498.

Lindzen, R. S., 1974: Wave-CISK in the tropics. *J. Atmos. Sci*., **31**, 156–179.

Liu C. and M.W. Moncrieff, 2004: Explicit simulations of the intertropical convergence zone. *J.Atmos. Science*, **61**, 458-473.

Liu C. and M.W. Moncrieff, 2008: Explicitly simulated tropical convection over idealized warm pools. *J. Geophys. Research*, **113**, D21121.

Liu Y., L. Guo, G. Wu, Z. Wang, 2010: Sensitivity of ITCZ configuration to cumulus convective parameterizations on an aqua planet. *Clim. Dyn.*, **34**, 223-240.

Mobis B. and B. Stevens, 2012: Factors controlling the position of the intertropical convergence zone on an aquaplanet. *J. Advances in Modeling Earth Sys.*, **4**, M00A04.

Neale R.B., et al., 2010: Description of NCAR community atmosphere model (CAM 4.0). Tech. Rep. NCAR/TN-485+STR, NCAR.

Neale, R. B., and B. J. Hoskins, 2000: A standard test for AGCMs including their physical parameterizations: I: The proposal. *Atmos. Sci. Lett.*, **1**, 101–107.

Neelin J.D. et al., 1992: Tropical air-sea interaction in general circulation models. *Climate. Dyn.*, **7**, 73-104

Numaguti A., 1993: Dynamics and energy balance of Hadley circulation and the tropical precipitation zones: significance of distribution of evaporation. *J.Atmos. Science*, **50**, 1874-1887.

O'Brien, T.A., F. Li, W.D. Collins, S.A. Rauscher, T.D. Ringler, M.A. Taylor, S.M. Hagos, L.R. Leung, 2013: Observed scaling in clouds and precipitation and scale incognizance in regional to global atmospheric models, *J.Climate*, in press

Oueslati B. and G. Bellon, 2012: Tropical precipitation regimes and mechanisms of regime transition: contrasting two aquaplanet general circulation models. *Climate. Dyn.*, DOI 10.1007/s00382-012-1344-x.

Rauscher S., T. Ringler, W.C. Skamarock and A.A. Mirin, 2012: Exploring a global multi-resolution modeling approach using aqua-planet simulations. *J. Climate*, doi: http://dx.doi.org/10.1175/JCLI-D-12-00154.1.

Ringler T., L. Ju, and M. Gunzburger, 2008: A multi resolution method for climate system modeling: Application of spectral centroidal Voroni tessellations. *Ocean Dynamics*, **58**, 475-498.

Ringler T.D., J. Thuburn, J.B. Klemp, and W.C. Skamarock, 2010: A unified approach to energy conservation and potential vorticity dynamics for arbitrarily structured C-grids. *Journal of Computational Physics*, **229**, 3065-3090.

Simmons, A. J., and D. M. Burridge, 1981: An energy and angular- momentum conserving vertical finite-difference scheme and hybrid vertical coordinates. *Mon. Wea. Rev.*, **109,** 758–766.

Skamarock, W.C., J.B. Klemp, M.G. Duda, L. Fowler, S.-H. Park, and T.D. Ringler, 2012: A multi-scale nonhydrostatic atmospheric model using centroidal voronoi tessellations and C-grid staggering. *Mon. Wea. Rev*., **240**, 3090-2105, doi:10.1175/MWR-D-11-00215.1.

Taylor, M.A., J. Edwards, and A. St. Cyr, 2008: Petascale atmospheric models for the community climate system model: New developments and evaluation of scalable dynamical cores. *Journal of Physics Conference Series*, **125** (1),012-023.

Thuburn, J., T.D. Ringler, W.C. Skamarock, and J.B. Klemp, 2009: Numerical representation of geostrophic modes on arbitrarily structured C-grids. *Journal od Computational Physics*, **228**, 8321-8335.

Tian, B., and V. Ramanathan, 2003: A simple moist tropical atmosphere model: The role of cloud-radiative forcing. *J. Climate*, **16**, 2086–2092.

Wheeler, M., and G. N. Kiladis, 1999: Convectively coupled equatorial waves: Analysis of clouds and temperature in the wavenumber– frequency domain. *J. Atmos. Sci*., **56**, 374–399.

Wilcox E.M., V. Ramanathan, 2001: Scale dependence of thermodynamic forcing of tropical monsoon clouds: results from TRMM observation. *J. Climate.*, **14**, 1511-1524.

Williamson, D.L., and J.G. Olson, 2003: Dependence of aqua-planet simulations on time step. *Quart. J. Roy. Meteor. Soc*., **129**, 2049-2064.

Williamson, D.L, 2008: convergence of aqua-planet simulations with increasing resolution in the Community Atmospheric Model, Version 3. *Tellus A*, **60 (5)**, 848-862.

Zhang, X.H., W.Y. Lin, and M.H. Zhang, 2007: Towards understanding the double intertropical convergence zone pathology in coupled ocean-atmosphere general circulation models. *J. Geophys. Res.*, **112**, D12102.

Zhang, G.J., and N.A. McFarlane, 1995: Role of convective scale momentum transport in climate simulation. *J. Geophy. Res.*, **100**, 1417-1426.

Zhang, G.J., and H. Wang, 2006: Toward mitigating the double ITCZ problem in NCAR CCSM3. *Geophysical Research Letters*, **33**, L06709.

Figure List

Figure 1. Zonal mean precipitation (ms^{-1}) in MPAS-A (left) and HOMME (right) corresponding to different resolutions. Color code given in the figure.

Figure 2. Zonal mean precipitation, advection and evaporation in M240 (left), M30 (center) and H28 (right) simulations.

Figure 3. Latitude – height distribution of zonal mean vertical pressure velocities in M240 (left), M30 (center) and H28 (right) simulations.

Figure 4. Zonal mean convective available potential energy ($J\ kg^{-1}$) in M30 (thick solid line), M30 (thin solid line) and H28 (dashed line)

Figure 5. Latitude – height distribution of difference in zonal mean temperature and specific humidity between H28 and M30 simulations

Figure 6. Zonal mean cloud fraction in M30 (left) and M240 (right) simulations.

Figure 7. Ratio of Kelvin wave amplitude to that of asymmetric Rossby and IG waves.

Figure 8. Zonal mean gross moist stability (K) at the equator for HOMME and MPAS-A simulations.

Figure 9. Schematic of the feedback mechanisms corresponding to double and single ITCZ simulations.

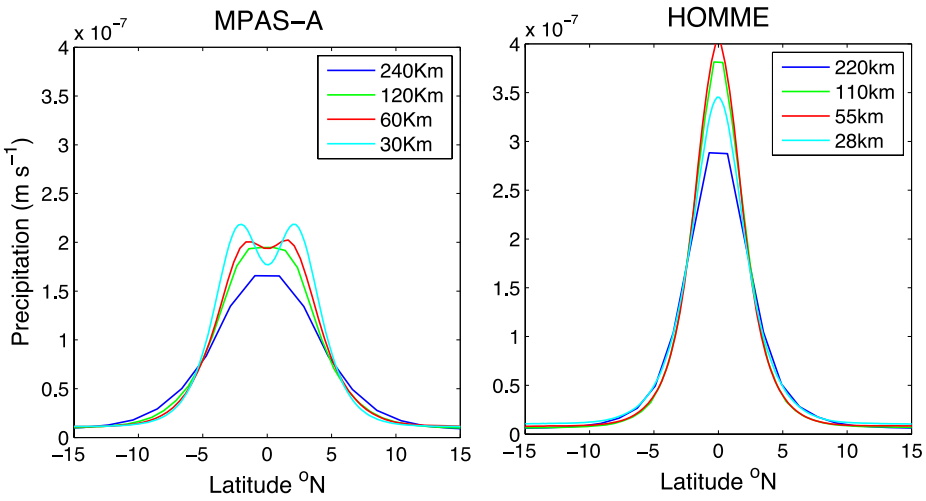

Figure 1. Zonal mean precipitation (ms^{-1}) in MPAS-A (left) and HOMME (right) corresponding to different resolutions. Color code given in the figure.

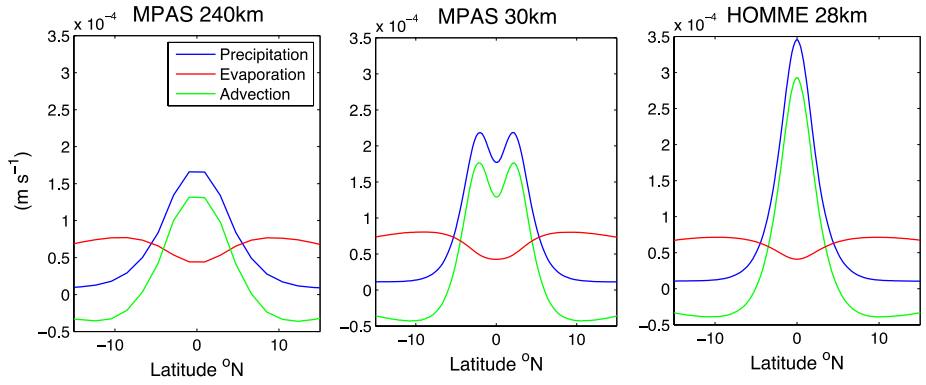

Figure 2. Zonal mean precipitation, advection and evaporation in M240 (left), M30 (center) and H28 (right) simulations.

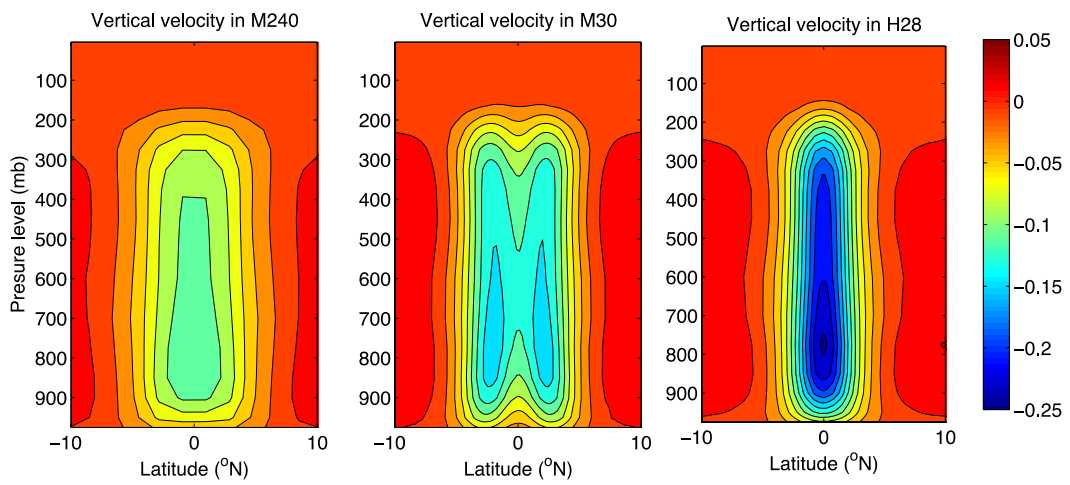

Figure 3. Latitude – height distribution of zonal mean vertical pressure velocities in M240 (left), M30 (center) and H28 (right) simulations.

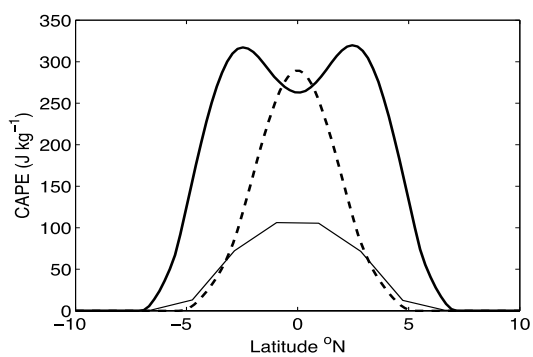

Figure 4. Zonal mean convective available potential energy (J kg^{-1}) in M30 (thick solid line), M240 (thin solid line) and H28 (dashed line)

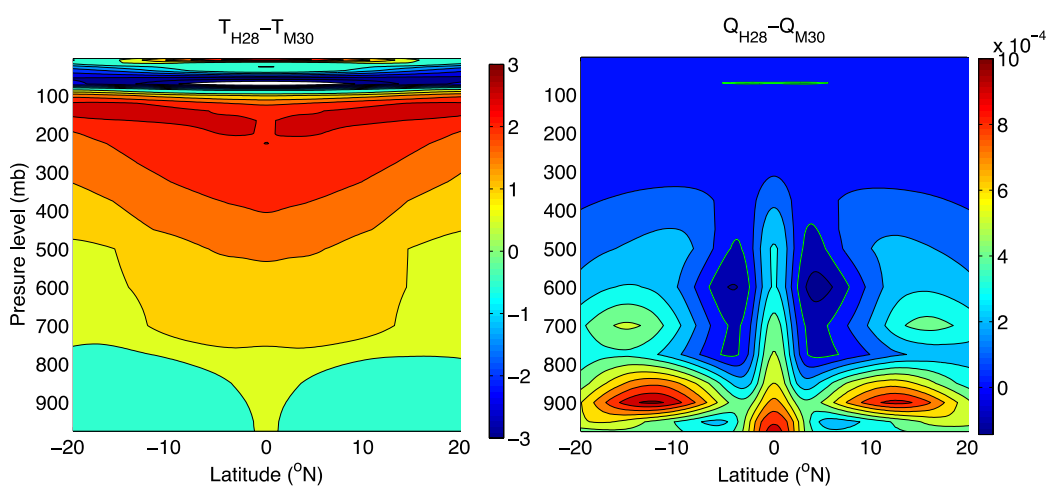

Figure 5. Latitude – height distribution of difference in zonal mean temperature and specific humidity between H28 and M30 simulations

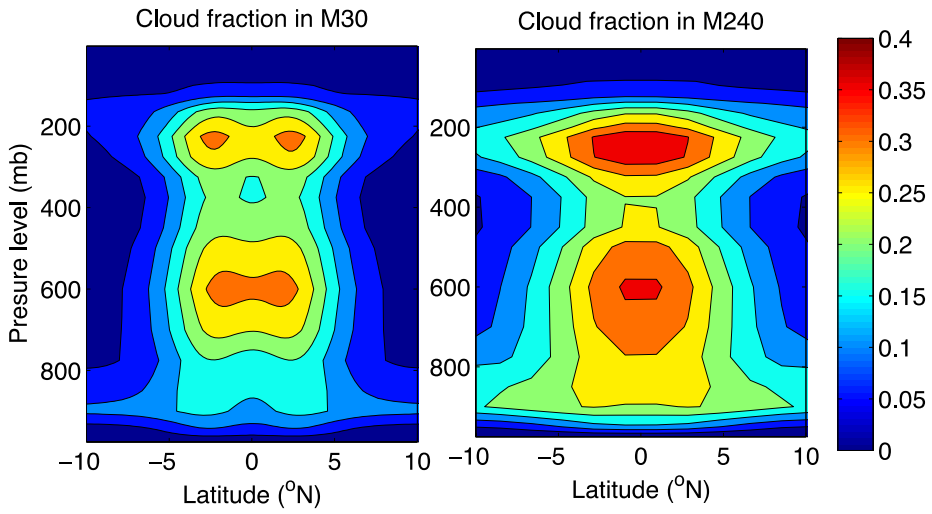

Figure 6. Zonal mean cloud fraction in M30 (left) and M240 (right) simulations.

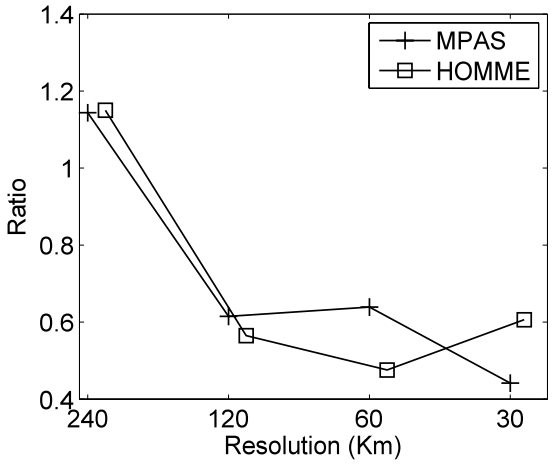

Figure 7. Ratio of Kelvin wave amplitude to that of asymmetric Rossby and IG waves.

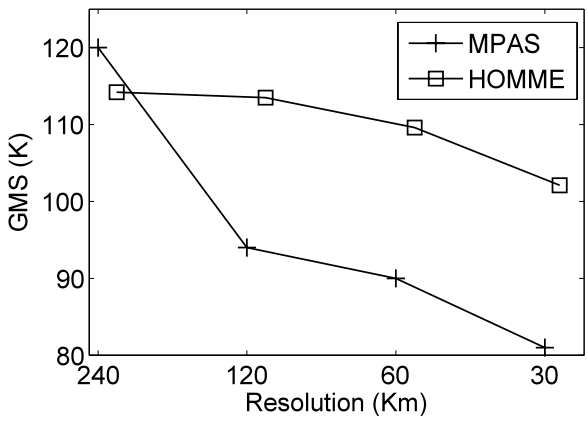

Figure 8. Zonal mean gross moist stability after dividing with C_p (in units of K) at the equator for HOMME and MPAS-A simulations.

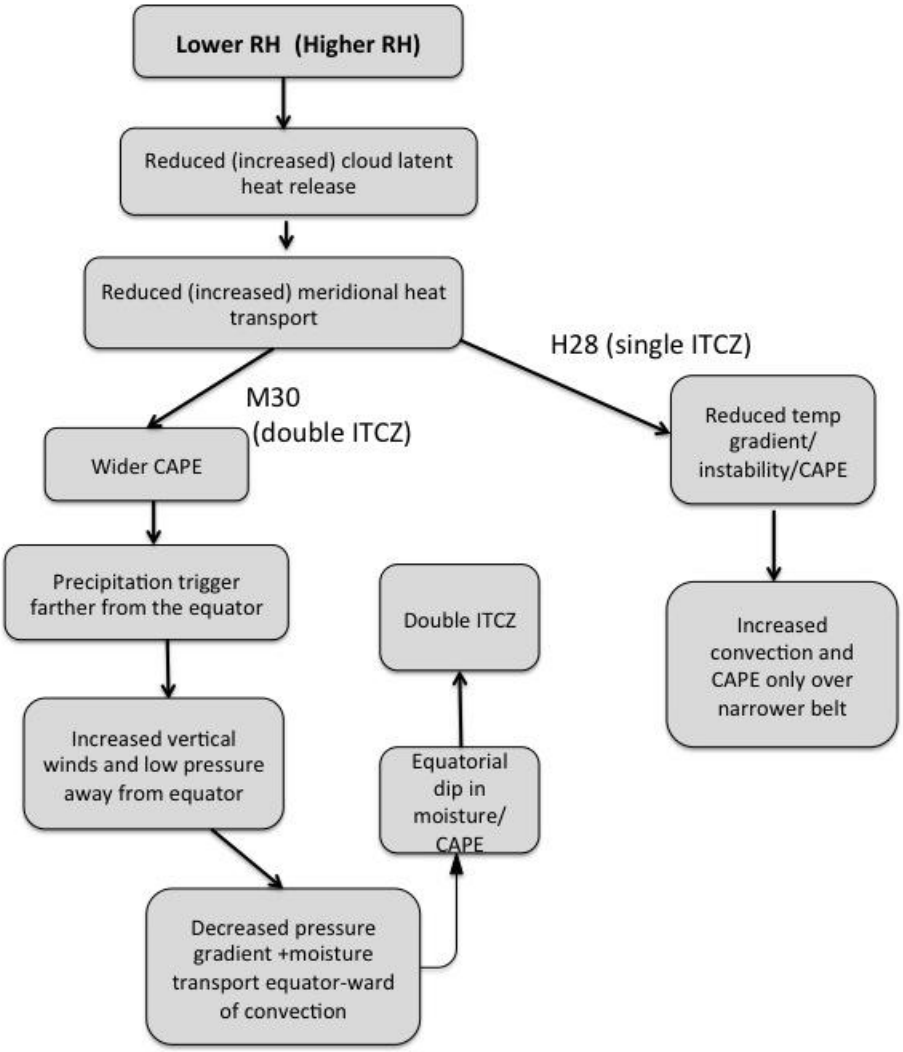

Figure 9. Schematic of the feedback mechanisms corresponding to double and single ITCZ simulations.